Cambridge University Press
978-1-107-40673-5 - Integrated Miniaturized Materials—From Self-Assembly to Device Integration: Materials Research Society Symposium Proceedings: Volume 1272
Editors: Carlos J. Martinez, Amit Goyal, Alberto Saiani, David Gracias and Rajesh R. Naik
Excerpt
More information

Micro- and Nanofluidic Systems for Material Synthesis, Device Assembly, and Bioanalysis

© in this web service Cambridge University Press

CAMBRIDGE

Cambridge University Press
978-1-107-40673-5 - Integrated Miniaturized Materials—From Self-Assembly to
Device Integration: Materials Research Society Symposium Proceedings: Volume 1272
Editors: Carlos J. Martinez, Amit Goyal, Alberto Saiani, David Gracias and Rajesh R. Naik
Excerpt
More information

Mater. Res. Soc. Symp. Proc. Vol. 1272 © 2010 Materials Research Society **1272-KK03-05**

Enhancement of on-chip bioassay efficiency with electrothermal effect

Kuan-Rong Huang, Jeng-Shian Chang, Sheng D. Chao, and Kuang-Chong Wu

Institute of Applied Mechanics, National Taiwan University, Taipei 106, Taiwan

ABSTRACT

We have performed the finite element simulations to study the binding reaction kinetics of the analyte-ligand protein pairs, C-reactive protein (CRP) and anti-CRP, in a reaction chamber of a biosensor. For diffusion limited reactions, diffusion boundary layers often develop on the reaction surface, thus hindering the reaction. To enhance the efficiency of a biosensor, a non-uniform AC electric field is applied to induce the electrothermal force which stirs the flow field. Biosensors with different arrangements of the electrode pairs and the reaction surface are designed to study the effects of geometric configurations on the binding efficiency. The maximum initial slope of the binding curve can be 6.94 times of the field-free value in the association phase, under an AC field of 15 V*rms* and an operating frequency of 100 *kHz*. With the electrothermal effect, it is possible to use a slower flow and save much sample consumption without sacrificing the performance of a biosensor. Several design factors not studied in our previous works such as the thermal boundary conditions are discussed.

INTRODUCTION

Immunoassay is a versatile biomedical diagnostic tool and provides a way for highly sensitive and precise detection of biological agents [1, 2]. The possibility of fabricating and integrating micro-sized biosensors with multiple functions has led to the idea of performing real-time monitoring or diagnostics on a portable lab-on-a-chip. Most biosensors employ the same kinetics of specific binding of analytes, such as C-reactive protein (CRP) [3], and immobilized ligands, such as anti-CRP. When the flow rate is fixed, the required experiment time of a specific bio-molecular recognition usually depends on its Damköhler number (*Da* number), which is the ratio of reaction velocity (i.e., product of the association rate constant and the initial concentration of the ligand) to the diffusion velocity (i.e., ratio of the diffusion coefficient of the analyte in the buffer flow to the height of micro-channel) [4]. When the *Da* number is greater than unity, the whole reaction is restrained by mass-transport process called diffusion limited reaction. This usually occurs in conditions of slow flow velocity in micro-channel, small diffusion coefficient of the analyte, and high association rate constant of reaction.

If the whole reaction is restrained by mass-transport, a diffusion boundary layer is often formed on the reaction surface [5, 6]. The formation of such layers would limit the response-time and the overall performance of a biosensor. In practice, it often takes hours to complete a detection cycle, which is the main technical problem to be solved. It is promising in our previous study [6] and the study of Sigurdson et al. [7] that several fabrication parameters can be tuned to improve the performance of a biosensor. From previous studies [8-19], the induced electrothermal force by the AC electric field can create a vortex field, called electrothermal flow, which will enhance the transport of the analyte to the reaction surface, reduce the thickness of the diffusion boundary layer and significantly increase the reaction rate to accelerate both the association and dissociation processes. However, these simulations were done only for two dimensional cases, limiting the spatial factors for practical designing. In this study, we will perform three dimensional simulations and study the effect of changing the relative geometrical

© in this web service Cambridge University Press www.cambridge.org

locations of the electrodes and reaction surface on the biosensor performance. The sample of CRP pairs in a biosensor immunoassay will be used to predict the surface concentration of the analyte-ligand complex versus time relationship.

THEORY

The details of the methodology used for the present 3D simulations are similar to our previous 2D simulations [6] and will be summarized briefly. This electrothermal force is given by [8]:

$$\vec{F_E} = -\frac{1}{2}\left[\left(\frac{\nabla\sigma}{\sigma} - \frac{\nabla\varepsilon}{\varepsilon}\right)\cdot\vec{E}\,\frac{\varepsilon\vec{E}}{1+(\omega\tau)^2} + \frac{1}{2}\left|\vec{E}\right|^2\nabla\varepsilon\right] \tag{1}$$

where $\tau=\varepsilon/\sigma$ is the charge relaxation time, ω is the angular frequency of the electric field $\vec{E}$, The electrostatic field $\vec{E}$ is related to the electrical potential Φ by :

$$\vec{E}=-\nabla\Phi \tag{2}$$

where Φ satisfies the Laplace's equation [20]

$$\nabla^2\Phi = 0 \tag{3}$$

The following energy balance equation must be solved [21].

$$\rho c_p\frac{\partial T}{\partial t} + \rho c_p\vec{V}\cdot\nabla T = k\nabla^2 T + \sigma\left|\vec{E}\right|^2 \tag{4}$$

where ρ, c_p, κ and $\vec{V}$ are the density, specific heat, thermal conductivity, and velocity of the fluid, respectively. In this work it is assumed that the fluid is incompressible so that

$$\nabla\cdot\vec{V} = 0$$

$$\rho\left(\frac{\partial\vec{V}}{\partial t} + \vec{V}\cdot\nabla\vec{V}\right) - \eta\nabla^2\vec{V} + \nabla p = \vec{F_E} \tag{5}$$

where η is the dynamic viscosity of the fluid and p is the pressure. Transport of analytes to and from the reaction surface is assumed to be described by the Fick's second law with convective terms:

$$\frac{\partial[A]}{\partial t} + \vec{V}\cdot\nabla[A] = D\nabla^2[A] \tag{6}$$

where $[A]$ is the concentration of analyte, and D is the diffusion coefficient of analyte in the fluid. The reaction between immobilized ligand and analyte is assumed to follow the first order Langmuir adsorption model [5, 22]. During the reaction, the analyte-ligand complex $[AB]$ increases as a function of time according to the reaction rate:

$$\frac{\partial[AB]}{\partial t} = k_a[A]_{surface}\left\{[B_0]-[AB]\right\} - k_d[AB] \tag{7}$$

where $[A]_{surface}$ is the concentration of the analyte at the reaction surface by mass-transport, $[B_0]$ is the surface concentration of the ligand, and $[AB]$ is the surface concentration of the analyte-ligand complex. Sketch of the 3-D model of the micro-channel is shown in Figure 1. In this work, the dimensions of the micro-channel and the reaction surface are $1000\mu m\times 500\mu m\times 100\mu m$ and

$200\mu m \times 40\mu m \times 3\mu m$, respectively. The dimensions of each electrode are 200 μm in length, 60 μm in width. The interval between the two electrodes is fixed at 60 μm.

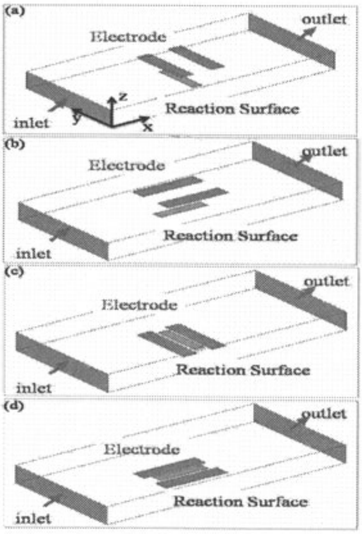

DISCUSSION

Fig. 1. The four arrangements of the electrodes and reaction surface.

The arrangements of the electrode pair and reaction surface

Figure 1 shows the four types of biosensors with different arrangements of the electrodes and reaction surface considered in this study. The applied voltage is 15 V and the inlet flow velocity is 100 μm/s. Table 1 lists the values of the initial slope and also the enhancement factors, defined as the ratio of the slope of binding reaction with applying electrothermal effect to that without applying electrothermal effect. Our previous study [6] revealed that the longer the length of the reaction surface along the flow direction is, the larger the diffusion boundary layer grows. The existence of the diffusion boundary layer on the reaction surface hinders the binding reaction of analyte-ligand pairs. Since Type-2/Type-4 biosensor has the longer dimension along the flow direction than Type-1/Type-3 biosensor does, the former is hindered more on the binding reaction than the latter. However, such geometrically caused hindrance can be removed by applying the external electrothermal field. The binding curve of Type-2 biosensor coincides almost with that of Type-1 biosensor after the electrothermal field is applied. Similar situation occurs for the Type-3 and Type-4 biosensors. It clearly suggests that the reaction surface should be put together with the electrodes at the same wall of the micro-channel to get better performance. Therefore the following simulations will focus on Type-3 and Type-4 biosensors.

Table 1The initial slopes and the enhancement factors for the four biosensors.

Type of biosensor	Initial slope (association) $\times 10^{-11}$	Initial slope (dissociation) $\times 10^{-11}$	Enhancement factor (association)	Enhancement factor (dissociation)
Type-1	2.30	-1.72	1.06	1.06
Type-2	2.21	-1.66	1.45	1.38
Type-3	4.42	-2.79	2.04	1.71
Type-4	4.51	-2.81	2.95	2.33

The thermal boundary conditions

Four cases of thermal boundary setting to the electrodes, and the top and bottom walls are considered in the simulation. For Case-1, the electrodes are controlled at 300 K, but both the top and bottom walls of the micro-channel are insulated. This is the case adopted in the above simulations. For Case-2, both the temperature of the electrodes and the bottom wall of the micro-channel are maintained at 300K but the top wall is insulated. For Case-3, both the temperature of the electrodes and the top wall of the micro-channel are maintained at 300K but the bottom wall is insulated. Finally, for Case-4, both the electrodes and the walls are all maintained at 300K. Moreover, the applied voltage is 15 V and the inlet flow velocity is 100 μm/s.

Table 2 Initial slopes and enhancement factors of the CRP binding reactions of Type-3/4 biosensor for the four cases of thermal boundary conditions.

Temperature boundary conditions	Initial slope (association) $\times 10^{-11}$	Enhancement factor (association)
Case-1 (electrodes at 300K)	4.43/4.52	2.03/2.93
Case-2 (electrodes and bottom wall at 300K)	4.05/4.37	1.86/2.84
Case-3 (electrodes and top wall at 300K)	3.80/4.04	1.75/2.62
Case-4 (electrodes, bottom wall and top wall at 300K)	3.73/4.08	1.72/2.65

Table 2 lists both the initial slopes and the enhancement factors for the association reaction for the Type-3/4 biosensor with the four different cases of temperature control. It is seen that the Case-1 temperature boundary setting produces the larger temperature rise and gradient around the reaction surface than the other three cases and turns out to yield the best performance among these four cases of the boundary temperature setting in terms of the initial slopes and enhancement of binding reaction,.

Effect of the inlet flow velocity

Table 3 shows the initial slopes and the enhancement factors in the association phase of the CRP binding reaction with various inlet flow velocities. It can be seen that higher flow velocity causes larger convective mass transport of the analyte and hence larger initial slope of the binding reaction. Nevertheless, the enhancement factor decreases monotonically as the inlet flow velocity increases. It means that the electrothermal effect is more efficient at lower inlet flow velocity than at higher velocity. For example, the enhancement factor is 6.94 for Type -4 biosensor when the inlet flow velocity is decreased to 5 μm/s, but only 1.25 for Type-3 biosensor when the inlet flow velocity is increased to 500 μm/s. Although the binding reaction rate for higher inlet flow velocity is still faster than the one for lower inlet flow velocity, the wasteful consumption of the sample is not worthy since most of them are carried away by the flow. Consider the Type-4 biosensor, with the inlet flow velocity and bulk concentration being 100 $\mu m/s$ and 6.4 nM, respectively. The saturation times t_{sat} for the binding reaction (not shown here) are about 1500s and 400s for 0 V and 15 V applied AC voltage, respectively. The

© in this web service Cambridge University Press www.cambridge.org

ratio of the bound analyte on the reaction surface to the total amount of the analyte supplied when the reaction is saturated can be computed as

$$\frac{[\mathrm{A}]_{\mathrm{sat}} \times \mathrm{Area}_{\mathrm{reaction\ surface}}}{[A]_{bulk} \times (A_{inlet} \times \mathrm{inlet\ velocity} \times t_{sat})} \approx \begin{cases} 0.17\% & \text{for } 0\ V \\ 0.63\% & \text{for } 15\ V \end{cases}$$

This simple calculation shows that the absorbed analyte is only less than 1 % of the total supplied samples and most of the samples go to waste. This ratio becomes even smaller when the inlet flow velocity becomes higher, say 500 $\mu m/s$.

Table 3 Initial slopes and enhancement factors in the association phase of Type-3/4 biosensor with Case-1 temperature condition for various inlet flow velocities.

w Velocity ($\mu m/s$)	Initial Slope $\times 10^{-11}$ (association), 0 V_{rms}	Initial Slope $\times 10^{-11}$ (association), 15 V_{rms}	Enhancement Factor (association)
5	0.14/0.14	0.77/0.98	5.41/6.94
10	0.63/0.52	2.20/1.99	3.46/3.81
30	1.34/1.01	3.99/3.82	2.97/3.77
50	1.68/1.23	4.32/4.34	2.57/3.53
100	2.18/1.53	4.42/4.51	2.04/2.95
300	3.10/2.13	4.48/4.61	1.45/2.17
500	3.59/2.46	4.49/4.67	1.25/1.90

In this respect, the advantage of applying electrothermal field is outstanding. It can efficiently raise the binding speed at lower inlet flow velocity to save the sample consumption without sacrificing too much the performance of a biosensor. We also observe that when no electrothermal field is applied, the performances of Type-3 and Type-4 biosensors are remarkably distinguished from each other. In fact, Type-3 biosensor has shorter dimension along the flow direction than Type-4 biosensor does, and hence has a smaller diffusion boundary layer zone than Type-4 biosensor does. The diffusion boundary layer hinders the binding reaction, as revealed in our previous study [6]. Thus Type-3 biosensor has better performance in binding reaction than Type-4 biosensor does. However, when the electrothermal field is applied, the diffusion boundary layers are almost completely eliminated for both Type-3 and Type-4 biosensors, and so this geometric effect to hinder the reaction rate is removed, and the binding reaction curves of Type-3 and Type-4 biosensors are quite close to each other now.

CONCLUSIONS

We study the electrothermal effect on the binding efficiency by performing three dimensional simulations on the immunoassay biosensor using the finite element analysis software, COMSOL Multiphysics $^{\mathrm{TM}}$ [23]. Our results indicate that the drawback of a longer reaction surface along the flow direction can be removed by applying the electrothermal force. A benefit of employing the electrothermal effect is that slower flow velocity in an immunoassay can be used to save sample consumption. Different boundary temperature controls can influence the binding rate significantly.

ACKNOWLEDGMENTS

This research was supported by the National Science Council in Taiwan through NSC 97-2221-E-002-017-MY3 and National Taiwan University CQSE 97R0066-69. We thank the NCHC in Taiwan for providing computing resources.

REFERENCES

[1] R. S. Yallow, and S. Berson, *Nature,* 184 (1959) 1648.
[2] P. A. Auroux, D. Iossifidis, D. R. Reyes, and A. Manz, *Anal. Chem.*, 74 (2002) 2637.
[3] W. S. Tillet, and T. Francis, *J. Exp. Med.*, 52 (1930) 561.
[4] W. M. Deen, *Analysis of Transport Phenomena*, Oxford University Press, New York, 1998.
[5] D. B. Hibbert, and J. J. Gooding, *Langmuir*, 18 (2002) 1770.
[6] C. K. Yang, J. S. Chang, S. D. Chao, and K. C. Wu, *J. App. Phys*, 103 (2008) 084702.
[7] M. Sigurdson, D. Wang, and C. D. Meinhart, *Lab on a chip*, 5 (2005) 1366.
[8] Ramos, H. Morgan, and A. Castellanos, *J.Phys.D:Appl.Phys.*, 31 (1998) 2338.
[9] R. Pethig, *Crit. Revs. Biotechnol.*,16 (1996) 331.
[10] Ramos, A. Gonzalez, N. Green, A. Castellanos, and H. Morgan, *Phys Rev.,* 61-4 (2000) 4019.
[11] N. Green, A. Ramos, A. Gonzalez, H. Morgan, and A. Castellanos, *Phys Rev.*, 61-4 (2000), 4011.
[12] C. Meinhart, D. Wang, and K. Turner, *Biomedical Microdevices,* 5-2 (2003) 139.
[13] X. B. Wang, Y. Huang, P. R. C. Gascoyne, and F. F. Becker, *IEEE Trans. Ind. Appl.,* 33 (1997) 660.
[14] H. Morgan, M. P. Hughes, and N. G. Green, *Biophysical J.,* 77 (1999) 516.
[15] M. Washizu, and S. Suzuki, *IEEE Transaction on Industry Application*, 30 (1994) 835.
[16] D. Wang, M. Sigurdson, and C. D. Meinhart, *Experiments in Fluid,* 38 (2005) 1.
[17] H. C. Feldman, M. Sigurdson, and C. D. Meinhart, *Lab on a chip*, 7 (2007) 1553.
[18] K. R. Huang, J. S. Chang, S. D. Chao, K. C. Wu, C. K. Yang, C. Y. Lai, S. H. Chen, *J. App. Phys*. 104 (2008), 064702.
[19] C. K. Yang, J. S. Chang, S. D. Chao, and K. C. Wu, *App. Phys. Lett.*,. 91 (2007), 113904.
[20] J. A. Stratton, *Electromagnetic Theory*, McGraw Hill, New York, 1941.
[21] L. D. Landau and E. M. Lifshitz, *Fluid Mechanics*, Pergamon, Oxford, 1959.
[22] Langmuir, *J. Am. Chem. Soc.*, 40 (1918) 1361.
[23] Comsol Multiphysics Version 3.4, COMSOL Ltd., Stokhelm, Sweden.

© in this web service Cambridge University Press www.cambridge.org

CAMBRIDGE

Cambridge University Press
978-1-107-40673-5 - Integrated Miniaturized Materials—From Self-Assembly to
Device Integration: Materials Research Society Symposium Proceedings: Volume 1272
Editors: Carlos J. Martinez, Amit Goyal, Alberto Saiani, David Gracias and Rajesh R. Naik
Excerpt
More information

Mater. Res. Soc. Symp. Proc. Vol. 1272 © 2010 Materials Research Society **1272-KK05-01**

Experimental characterization of the whipping instability of charged microjets in liquid baths

G. Riboux[1], A. G. Marín[1], A. Barrero[1], A. Fernández-Nieves[2] & I. G. Loscertales[3]

[1] Escuela Superior de Ingenieros, Universidad de Sevilla, Seville, Spain
[2] School of Physics, Georgia Institute of Technology, GA, USA.
[4] Escuela de Ingenierías, Universidad de Málaga, Málaga, Spain

ABSTRACT

Capillary liquid flows have shown their ability to generate micro and nano-structures which can be used to synthesize material in the micro or nanometric size range. For instance, electrified capillary liquid jets issued from a Taylor are broadly used to spin micro and nanofibers when the liquid consists of a polymer solution or melt, a process termed electrospinning. In this process, the electrified capillary jet may develop a non-axisymmetric instability, usually referred to as whipping instability, which very efficiently transforms electric energy into stretching energy, thus leading to the formation of extremely thin polymer fibers. Even though non axisymmetric instabilities of electrified jets were first investigated some decades ago, the existing theoretical models provide a qualitative understanding of the phenomenon but none of them is accurate enough when compared with experimental results. This whipping instability usually manifests itself as fast and violent lateral motion of the charged jet, which makes it difficult its characterization in the laboratory. However, this instability also develops when electrospinning is performed within a liquid bath instead of air. Although it is essentially the same phenomenon, the frequency of the whipping oscillations is much slower in the former case than in the latter, thus allowing detailed experimental characterization of the whipping instability. Furthermore, since the outer fluid is a liquid, its density and viscosity may now be used to influence the dynamics of the electrified capillary jet. In this work we present and rationalize the experimental data collecting the influence of the main parameters on the whipping characteristics of the electrified jet (frequency, amplitude, etc.).

INTRODUCTION

The electro-hydrodynamic (EHD) stretching of a liquid meniscus is among the most popular and versatile techniques to form extremely thin electrified capillary jets that may be used to synthesize various types of micro or nanoparticles [1]. This EHD technique is usually split into those used to produce spherical-like particles, termed electrosprays, and those used to form fiber-like particles, called electrospinning. In either case, an electrified conical meniscus, called Taylor cone, is formed at the tip of a capillary tube; from the tip of that cone, a thin electrified jet of liquid is issued. The nature of this phenomenon renders the charged jet unstable under axisymmetric (varicose) and non-axisymmetric perturbations. The former ones tend to break the jet into droplets with diameter of the order of the jet, similarly to what happens to uncharged jet break up, and so the processing of these airborne micro or nanodroplets gives rise to micro or nanoparticles. The non-axisymmetric instability, which do not appear in uncharged jets, manifest itself spontaneously as very fast and violent spiral-like and lateral motions of the jet; in this case, the electric energy is efficiently transferred into stretching energy and so, if the jet survives this

© in this web service Cambridge University Press www.cambridge.org

Cambridge University Press
978-1-107-40673-5 - Integrated Miniaturized Materials—From Self-Assembly to Device Integration: Materials Research Society Symposium Proceedings: Volume 1272
Editors: Carlos J. Martinez, Amit Goyal, Alberto Saiani, David Gracias and Rajesh R. Naik
Excerpt
More information

stressing motion, its diameter is dramatically thinned. This type of instability is called whipping instability and is responsible for the formation of nanofibers from polymer solutions or melts.

Since both types of instabilities are competing, it becomes naturally interesting to look for the parameters that determine which one grows faster in order to adjust the experimental parameters to produce either nanoparticles or nanofibers. Even though the work on electrospray and electrospinning has grown dramatically during the last decade, most of the literature on electrospinning deals with phenomenological studies testing the electrospinnability and properties of different polymer solutions, and only few works are devoted to theoretically predicting the behavior of the charged jet [2-4]. Some of the theoretical works qualitatively predict the dominance of either instability, or the expected final diameter of the electrospun fibers, but seldom describe in a detailed manner the dynamics of the whipping. It then seems appropriate to devote some effort to characterize the whipping. Unfortunately, this task becomes rather difficult mainly due to the very short characteristic times of this violent motion, which makes it extremely difficult to record or to photograph its evolution.

Recently, Barrero's group [5] operated an electrospray in steady cone-jet mode inside a dielectric liquid medium. Although electrosprays within a host liquid medium are ruled by the same physical principles than those operated in air, there are, however, some differences in their behaviors. For instance, the oscillations of the whipping instability are much less violent when the process is run inside a dielectric liquid than in air. This effect, due to the much larger value of the inertia of the outer fluid, results in jet oscillations at frequencies several orders of magnitude lower than those typically found in electrospinning in air [3, 6, 7]. Taking advantage of this damping effect, we have carried out an experimental characterization of the whipping instability of a charged capillary jet issued from an electrospray of glycerin operated within hexane (a dielectric liquid bath). To do so we have measured the whipping frequency, amplitude and wavelength in terms of the governing parameters, flow rate and electrical field.

EXPERIMENTAL

The experimental setup is entirely similar to that reported in previous works on electrosprays inside liquid media [4, 8]. It consists of an open tank of Plexiglas with a $38 \times 32\ mm^2$ cross-section and 180 mm high, see figure 1a. Two of the walls of the tank were made of glass to allow visualization. The tank was filled with hexane, whose viscosity, density and relative electrical permittivity were, respectively, $\mu_e = 0.3\ mPa.s$, $\rho_e = 660\ kg.m^{-3}$ and $\frac{\epsilon_e}{\epsilon_o} = 1.89$, where ϵ_e is the electrical permittivity of the hexane and ϵ_o is the vacuum permittivity. A round electrode-collector of $23\ mm$ of diameter connected to electrical ground was located at the bottom of the tank. A metallic needle of inner radius $a = 115\ \mu m$ immersed in the hexane was positioned at a fixed distance $H = 27\ mm$ above the collector. Glycerin was injected through the needle at a flow rate Q; a Harvard PHD 4400 programmable syringe pump with a Hamilton Gastight glass syringe of $32.6\ mm$ in diameter was used to control the flow rate. The physical properties of the glycerin were: density $\rho = 1250\ kg.m^{-3}$, dynamic viscosity $\mu = 1280\ mPa.s$, electrical conductivity $K = 1.7 \times 10^{-6}\ S.m^{-1}$ and electrical permittivity $\frac{\epsilon}{\epsilon_o} = 43$.

© in this web service Cambridge University Press www.cambridge.org